Data supplement for Cruceanu et al., Cell-Type-Specific Impact of Glucocorticoid Receptor Activation on the Developing Brain: A Cerebral Organoid Study. Am J Psychiatry (doi: 10.1176/appi.ajp.2021.21010095)

CONTENTS

Supplementary Results

A. Developmental characterization of organoids using bulk RNA sequencing and immunofluorescence confocal microcopy

Early progenitor markers PAX6 and NESTIN (*NES* gene) maintained consistent levels throughout organoid development. Basal progenitor markers TBR2 (*EOMES* gene) and HOPX progressively increased in expression across organoid maturation with significant peaks at day 158, likely reflective of increased neuronal maturation (**Figure 1B**, **Table S2**). Young neuronal marker MAP2 and mature neuronal markers TBR1 and CTIP2 (*BCL11B* gene) appeared later in organoid development but maintained constant levels as the organoids increased in age, from day 40 on with a significant peak at day 120 (**Figure 1C**, **Table S2**). Immunofluorescence staining in day 40 and day 90 organoids supported these findings at the protein level (**Figure 1D**). This cell-type distribution is consistent with a gradual maturing of the three-dimensional brain-like structure centered on the functional unit of the ventricle, with progenitors populating the apical surface of the ventricular zone and migrating toward the basal surface of the cortical plate as they differentiate.

B. Annotations of cell types based on marker genes in single-cell transcriptome data

All 17 identified cell clusters fit within three cell classes based on well-established markers(1-7) as follows (**Figure 3B**, **Figure 3C** inset table). Non-Neural Progenitors (n=2,274), representing the cells that have not been poised for a neuronal lineage differentiation, were characterized by

expression of epithelial marker *EPCAM* (**Figure S3**) and tight junction protein *OCLN*, as well as stromal markers *LUM* and extracellular markers like collagens *COL1A2*. Importantly, these cells do not express *PAX6* at high levels, which appears during the mesenchymal-to-epithelial transition from neuroepithelia to radial glia and is indicative of a commitment toward neuronal lineage. development. The cell types that contribute to the Non-Neural Progenitor cell class are the neuroepithelia (NE) being primarily made up of day 30 cells and distinctly expressing cell cycling markers *LIN28A* and *ASPM*, in addition to *OCLN* and *EPCAM*. The Epithelial Stromal cells (ES) cluster distinctly expresses a combination of early markers *EDN1* (endothelial), *CD68* (associated to microglia and other peripheral cells), *TSTD1*, *CDH1*, all of which have been shown by other groups to be associated with neuroepithelial cells (**Figure 3B; Figure S3**). Finally, the Mesenchymal cells (M) which express structural proteins like *LUM* and *DCN* and collagens like *COL1A2*, and the Endothelial cells (E) which express *EDN1*, round out this cell class.

The second cell class represents the Neural Progenitors (n=7,576 cells), defined by appearance of *PAX6* (**Figure 3C-D; Figure S3**), and consisting of 5 clusters including most notably Glial Precursors (GP) which express oligodendrocyte precursor as well as astrocyte marker *S100B* and glial precursor transcription factor *SOX10*; Proliferative Precursors (PP) defined by expression of cycling markers *TOP2A*, *MIK67*, *ASPM*; Early Progenitors / Neuronal Precursors (EP) which express progenitor markers *VIM* and *PAX6* as well as neuronal lineage markers *NES*, *NCAM1*; and Radial Glia (RG) expressing markers *PAX6*, *SOX2*, *HES1*, *HES5*, and *CDH2* (**Figure 3B; Figure S3**). This is the most inclusive and heterogeneous class of cells, showing the potential of organoid-derived progenitor cells to differentiate into the majority of cell types present in the human brain. However, their abundance also highlights the early stage of development modeled in this system.

The third cell class represents the Neurons (n=4,152 cells) and is defined by expression of neuronal markers *STMN2* and *DCX* (**Figure 3C-D; Figure S3**). It includes the most immature and heterogeneous immature Neurons (iN) which express *MAP2*, *DCX*, some dorsal markers like *NEUROD1* and *NEUROD4* as well as ventral marker *OTX2*, but also some retinal markers like *CRX* and *RCVRN*. In spite of some ventral markers present, our organoids primarily seem to differentiate along a dorsal lineage, with the immature Dorsal Neurons (iDN) expressing *MAP2*, *DCX*, and some dorsal-specific *NEUROD6* and the most differentiated Dorsal Neurons (DN) expressing *NEUROD6* abundantly, as well as glutamatergic receptor *GRIA2* and synaptic protein *SNAP25* (**Figure 3B; Figure S3**).

C. Cell-type distribution in cerebral organoids across developmental time shows neuronal maturation

When separating cells by developmental time-point, by-and-large the same cell-types were represented and identified by the same markers, with the main difference being relative cell abundance (**Figure 3C; Figure S3A-C**). For example, the proportion of Neuroepithelial cells (NE) decreased as the organoids aged (Chi-square=15.58, p-value=0.0004) while the proportion of more differentiated cell-types like the Dorsal Neurons (DN) increased (Chi-square=6.03, p-value=0.049) (**Figure 3C**).

Even more prominently than with individual cell-types, the percent of cells in each cell class across organoid age changed with maturity. Non-Neural Progenitors decreased from 26% at day 30 to

12% cells at day 60 and 9% at day 90 (Chi-square=12.5, p-value=0.002) while there was not significant change in Neural Progenitors (p-value=0.75), with this class covering just above 50% of cells at all ages. Neurons increased progressively with organoid age from 19% to 32% to 39% of cells at day 30, day 60, and day 90, respectively (Chi-square=9.8, p-value=0.007; **Figure 3D**).

D. Cell-type specific glucocorticoid response in organoids is GR-dependent

Since glucocorticoid-response has previously been established by our group and others in different tissue types like peripheral blood cells(8) as well as more recently neuronal cell types like hippocampal progenitors(9), we wanted to test the overlap of these previous findings with our results from GC-exposure in organoids. We first tested whether the effects we observed following glucocorticoid exposure were dependent on expression of the glucocorticoid receptor (*NR3C1* gene). We found that cells with sufficient mRNA levels of *NR3C1* and thus positive for this gene's expression in our data, displayed significantly higher absolute fold changes in all three cell classes (p-value <0.0001) compared to *NR3C1*-negative cells after Dex treatment (**Figure 4H**). This fold-change distribution was tested in a set of genes that was previously determined to be indicative of glucocorticoid-response in a human hippocampal progenitor cell line following a similar acute stimulation paradigm(9). This supports the notion that the observed Dex-response phenotype of individual cells is indeed mediated via cell-intrinsic GR.

E. Cell-type-specific differential expression in fine clusters defined by scRNAseq

At the 17-cluster level, we found significant differentially-expressed genes (DEGs) in 9 clusters, ranging from one to 55 DEGs (q-value≤0.05; **Figure 5A**, **Table S8**). Radial Glia (RG) had the most significant DEGs (n=55) followed by the immature Dorsal Neurons (iDN, n=47 genes), the Dorsal Neurons (DN, n=38 genes), and the Proliferative Progenitors (PP, n=37 genes) (q-value≤0.05; **Figure 5A**, **Table S8**). No gene was DE in more than four clusters, but 5 genes were shared among the four clusters with most DEGs (PP, RG, iDN, and DN) (**Figure 5B**). Of these, *MGARP* was up-regulated, while *C1orf61*, *LINC01551*, *NEUROD6*, and *NFIA* were down-regulated by Dex. The direction of DE fold-change (FC) was consistent across all three time-points (**Tables S5-7**), indicating a cell-type and not temporally-dependent effect. Genes associated with neuronal phenotypes like *NEUROD6*, *C1orf61*, and *NFIA* were among the most strongly down-regulated in multiple clusters (**Figure 5B** inset table for FC). The DN cluster exhibited the largest FCs, with the top 6 ranked transcripts by p-value displaying absolute FC above 2.0 (**Table S8**). Interestingly, all these transcripts were down-regulated by Dex, and included *NEUROD6*, *C1orf61*, *NFIA*, and *NFIB*, suggesting possible disruptive effects of GR-activation on neuronal differentiation and maturation, however power in this 17-cluster DEG analysis was limited.

F. Enrichment of Intellectual Disability-associated genes carrying loss-of-function mutations in coarse cells classes from Line1 organoids

To assess the impact of genetic mutations in neurodevelopmental disorders among the genes we found DE in our case-control comparisons, we tested enrichment against a gene list focusing

specifically on genes carrying loss-of-function mutations associated with ID from the Developmental Brain Disorders Database (DBDD)(10) (gene list in **Table S13**). We started with the DEGs from the coarse cell-class groupings. When testing for enrichments within genes with ID-related loss-of-function mutations in DBDD, we found a highly significant enrichment of DEGs in Neurons only (q-value=$5.97x10^{-8}$; OR=5.6, **Figure S5B**; **Table S13**), finding which proved to be driven by GR-activation, with 0 of 1,000 permuted iterations of the test gene list reaching p-value≤ the nominal p-value (**Figure S5B**; **Table S13**). This enrichment was based on 17 DEGs mapping to ID-associated genes with loss-of-function mutations, including the *NRXN1, TCF4, TBR1* and *PAX6* genes where multiple pathogenic mutations have been linked to neurodevelopmental disorders. When breaking the analysis down by 17 cell-types, this result was consistent and even more pronounced in the most mature cell cluster, the Dorsal Neurons (q-value=$5.05x10^{-8}$, OR=25.80; permutation-based empirical q-value=0.004; **Table S13**).

Supplementary Materials and Methods

I. hiPSCs and Organoids

Line 1 induced pluripotent stem cells were derived via reprogramming from NuFF3-RQ human newborn foreskin feeder fibroblasts, male (GSC-3404, GlobalStem)(11). Line 2 cells were generated using a plasmid-based protocol for derivation of integration-free human iPSCs from peripheral blood mononuclear cells(12) from a female donor collected at the Max Planck Institute for Psychiatry through the BeCOME study(13). Line 3 hiPSCs were reprogrammed from a female donor's skin fibroblasts (HPS0076- 409b2, RIKEN BRC cell bank)(14, 15). All hiPSCs were cultured on 6-well plates (Thermo Fisher) coated with 1:30 Matrigel (Corning) in mTesR1 basic medium supplemented with 1x mTesR1 supplement (Stem Cell Technologies) at 37°C, with 5% CO_2. Cerebral organoids (COs) were generated as previously described(16), starting with 9,000 hiPSCs dissociated into single cells using StemPro Accutase Cell Dissociation Reagent (Life Technologies) per each well in U-shaped low attachment 96-well tissue culture plates (Corning) in hES medium (DMEM/F12-GlutaMAX supplemented with 20% Knockout Serum Replacement, 3% FBS, 1% Non-essential amino acids, 0.1 mM 2-mercaptoethanol, 4 ng/ml bFGF and 50 µM Rock inhibitor Y27632) for 6 days in order to form embryoid bodies (EBs). On day 6, EBs were transferred into low attachment 24-well plates in Neural Induction (NIM) medium (DMEM/F12 GlutaMAX-supplemented with 1:100 N2 supplement, 1% Non-essential amino acids and 5 µg/ml Heparin) and cultured for an additional 6 days. On day 12 EBs were embedded in Matrigel (Corning, 354234) drops and transferred to 10-cm tissue culture plates in Neural Differentiation medium (NDM) without Vitamin A medium (DMEM/F12GlutaMAX and Neurobasal in ratio 1:1 supplemented with 1:100 N2 supplement 1:100 B27 without Vitamin A, 0.5% Non-essential amino acids, insulin 2.5 µg/ml, 1:100 Antibiotic-Antimycotic and 50 µM 2-mercaptoethanol) in order to form organoids. 4 days after Matrigel embedding, organoids were transferred into an orbital shaker and cultured in NDM with Vitamin A (DMEM/F12GlutaMAX and Neurobasal in ratio 1:1 supplemented with 1:100 N2 supplement 1:100 B27 with Vitamin A, 0.5% Non-essential amino acids, insulin 2.5 µg/ml, 1:100 Antibiotic-Antimycotic and 50 µM 2-mercaptoethanol).

Organoids were grown in these conditions at 37°C with 5% CO_2 until collection for RNA extractions, cryopreservation, or single-cell dissociation.

II. Glucocorticoid stimulation

Our primary intention in the experiments described here was to model clinical sGC exposure using dexamethasone (Dex), a synthetic glucocorticoid known to bind preferentially to the GR, though not exclusively. While Dex can activate the GR at much lower concentrations *in vitro*(17), the doses recommended to pregnant mothers consist of 24mg Dexamethasone phosphate given as 4 intramuscular injections at 12 hourly intervals. A single 6mg dose would reach a Cmax of 65–95 ng/ml at Tmax 3 hours (18), which would equal to a concentration of ~165-242nM from a single dose and as high as 968nM over the treatment duration, depending on how fast this is processed by the system. The maternal/fetal blood concentration ratio has been reported to be anywhere from 0.4 to 1 days after administration (18-21), so we would expect at the very least that the fetus could be exposed to concentrations of 66-968nM. Even if there are differences related to size of the mother or fetus further altering these ratios, these should not make a great impact on the amount of compound reaching different tissues, as synthetic GCs like Dex are known to pass through placental membranes.

Organoids of different ages depending on experiment were treated with glucocorticoids (GCs) by dissolving Dexamethasone (Dex) to the appropriate concentration (10nM, 100nM, or 1000nM) in DMSO and subsequently in the culture medium. 4 hours or 12 hours exposure time was employed, and all exposures were performed in triplicate experiments.

For long-term effects of acute glucocorticoid exposure, a 12-hour treatment of 100nM Dex or Vehicle (DMSO) was administered and whole organoids were collected and snap-frozen, followed by RNA extraction and qPCR analyses with candidate genes. The time points for organoid collections were as follows: 12 hours (immediately after exposure), 2 days, 6 days, and 8 days following the single acute exposure (during which time the organoids were kept in normal conditions). For immunohistochemistry and cell counting experiments, only the 8-day wait period was used and organoids were fixed and stained as in the following section.

III. Immunofluorescence

Organoids were fixed using 4% paraformaldehyde for 45 minutes at 4^{o}C, cryopreserved with 30% sucrose, fixed in optimal cutting temperature (OCT) compound (Thermo Fisher Scientific) and stored at -20^{o}C prior to cutting 16 um cryosections. For immunofluorescence, sections were post-fixed using 4% PFA for 10 mins and permeabilized with 0.3% Triton for 5 mins. Sections were subsequently blocked with 0.1% TWEEN, 10% Normal Goat Serum and 3% BSA. Primary and secondary antibodies were diluted in blocking solution, and fluorescent staining was visualized and analyzed using a Leica laser-scanning microscope. For staining with PAX6 and SATB2 the slides were put through antigen retrieval before fixing with paraformaldehyde. More specifically,

the slides were incubated with citric buffer (0.01 M, pH 6.0) for 1 min at 720 Watt and 10 mins at 120 Watt, left to cool down at room temperature for 20 mins and washed once with PBS.

Antibodies

Antigen	Dilution	Vendor	Catalog #
DAPI	1:1000	Sigma Aldrich	D9542
PAX6	1:500	Biozol	BLD-901301
SOX2	1:500	Cell Signaling	2748
HOPX	1:1000	Santa Cruz	HPA030180
CTIP2	1:500	Abcam	ab18465
SATB2	1:500	Abcam	Ab51502
TBR1	1:500	Abcam	ab31940
MAP2	1:500	Sigma Aldrich	M4403
TBR2	1:500	Abcam	ab23345
NESTIN	1:500	Santa Cruz	sc23927
GR (D8H2)	1:100	Cell Signaling	3660S

IV. Cell counting

a. GR-positive cells

To determine the cell compartment localization of GR-positive cells, multiple IF images (at 40x magnification) were scored for either vehicle (DMSO; n=7 pictures) or treated (100nM Dex; n=9 pictures). Cells were counted as having either nuclear-only (referred to as 'nuclear') or a combination of cytoplasmic and nuclear (referred to as 'both') GR protein staining. Roughly 1000 cells were counted in each condition, and statistical analyses were performed on percentage values using Chi-square tests with Yates correction.

b. Neuronal layer markers

To determine the abundance of TBR1-positive, CTIP2-positive and SATB2-positive neurons in organoids treated with 100nM Dex or Vehicle followed by an 8-day waiting period, multiple IF images of ventricles (at 25x magnification) were taken (n=17-21 ventricles for each marker, either Dex or Veh). The ventricle and cortical plate were marked based on DAPI-positive nuclei organization, and neuron-marker-positive cells were counted only within each ventricular zone only. Cell counts were normalized to the ventricular zone surface area, and group differences were computed using unpaired t-tests.

V. Bulk RNA sequencing

Organoids (following 17, 23, 40, 70, 120, 140, or 158 days in culture) were collected for bulk RNA extractions using the RNeasy Mini extraction kit (74104, Qiagen) according to the manufacturer's instructions. RNA quality and concentrations were measured on an Agilent 2100 Bioanalyzer (Agilent). Three replicates were analyzed per time point, every sample containing 1-3 pooled organoids. Sequencing libraries were prepared from a starting amount of 100ng total RNA using the NEBNext® Ultra™ DNA Library Prep Kit for Illumina (E7370L, New England Biolabs) using ribosomal depletion as a selection method, and sequenced paired-end on an Illumina HiSeq4000 system at the Helmholtz Zentrum Core Facility (Munich, DE). 5 libraries were pooled per lane for a total coverage of on average 50 M reads/library. Raw reads were processed using FastQC(22) and cutadapt(23) and aligned using the STAR aligner(24). The counts data were batch-corrected, normalized and analyzed and using the ImpulseDE2 framework(25). For practical representation in the heatmap (**Figure 1**), all genes were normalized to 1. Individual genes were plotted using GraphPad Prism V6 using log2-transformed values and mean ± standard deviation.

To confirm the developmental specificity of our cerebral organoid data, we integrated bulk gene expression data with several transcriptional data sets from human post-mortem brain tissue and other hiPSC-derived models. We used a recently described approach to integrate these data(26, 27). In brief, a total of 15 independent studies were analyzed covering 2,716 independent samples and 11,572 genes. These studies span a broad collection of developmentally specific gene expression, covering expression related to hiPSCs, hiPSC-derived NPCs, hiPSC-derived neurons, bulk prenatal brain tissue (early, mid and late fetal stages) as well as bulk postnatal brain tissue (early, mid and late stages). All expression values were converted to $\log_2$ RPKM and collectively normalized using quantile normalization from the *limma* R package(28). These data, along with our bulk cerebral organoid expression data were projected into a low-dimensional space using singular value decomposition analysis. The first two principal components were used to depict developmental trajectories.

VI. Quantitative Real-time Polymerase Chain Reaction (qRT-PCR)

Total RNA was extracted from organoids using the RNeasy Mini extraction kit (74104, Qiagen) according to the manufacturer's instructions. Complementary DNA (cDNA) synthesis was performed using the Maxima H Minus Reverse Transcriptase (Thermo Fisher) along with oligo(dT)16 primers (Invitrogen) and random hexamers (IDT DNA) in a 1:1 ratio. Real-time PCR reactions were run in quadruplicate using PrimeTime qPCR Primer Assays (IDT DNA) and PrimeTime® Gene Expression Master Mix (IDT DNA) on an ABI PRISM 7900HT Sequence Detection System (Applied Biosystems) or a LightCycler 480 Instrument II (Roche). Relative gene expression levels were quantified using the absolute quantification method, and using *GAPDH*, *POLR2A* and *YWHAZ* as endogenous genes. Statistical differences between groups were analyzed by Two-Way repeated measures ANOVA with Dunnet's post-hoc multiple comparisons tests. Statistical significance was calculated, and graphs were plotted using GraphPad Prism 7. A p-value

of ≤0.05 was considered statistically significant and marked as *, and ≤0.1 was considered suggestive of a trend for significance and marked as # in graphs.

Gene ID	Gene name	PrimeTime Assay
SOX2	SRY (sex determining region Y)-box 2	Hs.PT.58.237897.g
PAX6	Paired box protein Pax-6	Hs.PT.58.38519242
MAP2	Microtubule-associated protein 2	Hs.PT.58.20103440
TUBB3	Class III β-tubulin	Hs.PT.58.20385221
NR3C1	Glucocorticoid Receptor	Hs.PT.58.27480377
FKBP5	FKBP prolyl isomerase 5; FK506 binding protein 5	Hs.PT.58.20523859
SGK1	Serum and glucocorticoid-regulated kinase 1	Hs.PT.58.19153459.gs
TSC22D3	GILZ; glucocorticoid (GC)-induced leucine zipper	Hs.PT.58.4331913
ZBTB16	Zinc finger and BTB domain containing 16	Hs.PT.58.605743
MGARP	Mitochondria localized glutamic acid rich protein	Hs.PT.58.41038142
GAPDH	Glyceraldehyde 3-phosphate dehydrogenase	Hs.PT.39a.22214836
POLR2A	RNA Polymerase II Subunit A	Hs.PT.39a.19639531
YWHAZ	Tyrosine 3-Monooxygenase/Tryptophan 5-Monooxygenase Activation Protein Zeta	Hs.PT.39a.22214858

VII. Single-cell RNA sequencing

a. Data collection

Whole organoids (after 30, 60, or 90 days in culture) were treated with Dex (100nM) or Vehicle (DMSO) for 12 hours until harvesting for single-cell preparation. Single cells were dissociated using StemPro Accutase Cell Dissociation Reagent (Life Technologies), filtered through 30uM and 20uM filters (Miltenyi Biotec) and cleaned of debris using a Percoll (Sigma, P1644) gradient. Single cells were resuspended in ice-cold Phosphate-Buffered Saline (PBS) supplemented with 0.04% Bovine Serum Albumin and prepared for single-cell separation. All experiments in organoids from Line 1 hiPSCs were performed in quadruplicate at all three time points, with a paired design of a treatment (Dex) or control (Veh) condition per each experiment/iCell8 chip, for a total of 12 chips, using the iCELL8 Single-Cell System (Wafergen, Takara Bio) according to the manufacturer's recommendations. Briefly, cells were stained with Propidium Iodide (for dead cells) and DAPI (for live cells) on ice for 5-10 minutes and dispensed in the loading plate. Following microfluidic separation, iCell8 chips were imaged using the built-in fluorescence microscope and snap-frozen and stored at -80^{o}C until library preparation. Based on fluorescence labeling, only wells containing live single cells were selected for library preparation, which was performed according to the manufacturer's guidelines using the iCell8 Chip and Reagent Kit using in-chip RT-PCR amplification chemistry (Wafergen, Takara Bio) and Nextera XT DNA Library Preparation Kit and Nextera XT Index Kit (Illumina). All experiments from Line 2- and Line 3-derived organoids were performed at day 90 in quadruplicate in a pair-wise design with a treatment (Dex) or control (Veh) condition ran in parallel. Single cells were run through the Chromium

controller to form gel emulsion beads containing barcoded single cells and prepared into single-cell libraries using the Chromium Single Cell 3' Reagent Kits v2 according to the manufacturer's recommendations without any modifications (10X Genomics). All libraries were assessed using a High Sensitivity DNA Analysis Kit for the 2100 Bioanalyzer (Agilent) and KAPA Library Quantification kit for Illumina (KAPA Biosystems), and sequencing was performed paired-end with 26nt/100nt configuration on an Illumina HiSeq4000 system at the Helmholtz Zentrum Sequencing Core Facility (Munich, DE).

b. Data Analysis

b.1. Pre-processing and quality control of single-cell RNAseq data

Sequencing of the iCell8 single cell libraries (from Line 1-derived hiPSCs) was performed on an Illumina HiSeq4000 (Illumina, San Diego, CA), 1 lane per chip, generating paired-end reads of 100 bp length. The initial quality check was performed using FastQC(22) before demultiplexing the cells by their barcode with *Je* multiplexer version 1.0.6(29) requiring a perfect match of the sequence. Subsequent adaptor trimming was performed using cutadapt version 1.11(30). For read alignment, the STAR module(24) of the Cell Ranger 2.1.1 release with the corresponding reference index of GRCh38 version 1.2.0 was used, both provided by 10x Genomics. Only uniquely aligned reads with a minimum overlap of 31 bp to the transcriptome were regarded for gene quantification with the featureCounts package version 1.6.4(31). We converted Ensemble Gene IDs to Gene Symbols using the R package BED(32) with database version UCB-Human 2019.10.11.

Sequencing of the 10x Genomics single-cell libraries (from Line2- and Line3-derived organoids) was performed on an Illumina NovaSeq (Illumina, San Diego, CA), generating paired-end reads of 100 bp length. Count matrices were obtained from the fastq-files using Cell Ranger v3.0.2 with the transcriptome hg38_ensrel94.

We carried out all downstream analyses using the python-based Scanpy package(33) (https://github.com/theislab/scanpy) unless stated otherwise. To remove low quality cells in the iCell8 data, we filtered cells with a high fraction of reads from mitochondrial genes (20% or more - indicating stressed or dying cells), cells with <2,000 or > 600,000 total reads, as well as cells expressing < 600 genes. We also removed cells that were labelled as empty wells as part of the iCell8 library preparation procedure. In addition, we excluded genes with expression in < 20 cells. When analysing cells from one of the three time-points of the iCell8 data separately we removed all genes with expression in < 10 cells of the time-point in question. Unless stated otherwise, we carried out all following analyses with cells from all time-points of the iCell8 data combined as well as separately for each of the three time-points (day 30, 60 and 90).

Given the overall higher quality and sensitivity of the 10x data, more stringent filters for lower quality cells were applied here. Cells with a high fraction of reads from mitochondrial genes (25% or more - indicating stressed or dying cells), cells with <1,200 or > 150,000 total reads, as well as

cells expressing < 700 genes were removed from the expression matrix. All genes which were expressed in less than 20 cells of the total data were also removed from the expression matrix.

b.2. Normalisation and batch correction

To approximate the effect of sequencing depth in the data, we used the *computeSumFactors()* function from the R package scran(34). To remove this effect, we divided the reads of each cell by its associated size factor as computed by scran. We log-transformed the data and used the resulting expression matrix for computing marker genes as well as for differential expression analysis downstream. For the 10x data, we also used this log-normalised version of the data as input for any visualisations (both computing low-dimensional embeddings as well as visualising expression levels of individual genes).

For the visualisation of expression levels of individual genes form the iCell8 data, we removed technical variation introduced by handling of the different iCell8 chips using the Scanpy implementation of the combat package(35). For improved interpretability of plots representing gene expression, we limited colour scales and axis limits to combat-corrected expression values between 0 and 8. This ensures comparability between the visualisation of the expression values of different genes prevents outlier cells with extremely high expression values from dominating visualisations and also ensures that negative expression values produced by combat are not affecting visualisations.

The small positive and negative expression values introduced by combat in places of zero gene expression are particularly problematic when relying on dot plots to visualise the expression of marker genes. While this behaviour is a natural result of the underlying regression approach combat uses to remove technical variation, this result is not compatible with a dot plot as a marker gene visualisation tool. This is because the concept of a dot-plot relies heavily on the absence of expression of a gene in all but a few cells. In order to ensure compatibility between combat-correction and dot plot visualisations of marker genes, we adjusted the expression matrix in the following way: (1) we computed the median expression of each gene after combat correction while excluding all values from the median calculation that were zero before combat correction; (2) we set all entries in the post-combat expression matrix to zero which were zero before combat correction and at the same time were below the previously computed median expression value of the respective gene. This way, we only allowed combat to activate the expression of genes if the combat-corrected expression value was above the median expression value of that gene. On the one hand this prevents combat to turn on expression of spurious genes by a small amount and on the other hand still allows for turning on gene expression if the batch effect dominates the expression of a particular gene.

In order to obtain a meaningful low-dimensional embedding of the iCell8 data, we carried out a separate normalisation and batch correction step starting again from the raw count data as before. We used a negative binomial generalised linear regression model with regularised over-dispersion

parameter theta, as introduced in(36), with the iCell8 chip ID as a batch covariate. To this end we used the R function *norm.nb.reg( )* from the github repository associated with(36) (https://github.com/ChristophH/in-lineage). We constructed the normalised expression matrix from the Pearson residuals of the regression model.

b.3. Low dimensional embedding, visualisation and clustering

We computed the single-cell neighbourhood graph on the 50 first principal components of the negative binomial residuals' expression matrix using 15 nearest neighbours. We used Uniform Manifold Approximation and Projection (UMAP)(37) for visualising the data in two dimensions. For clustering and cell type identification we used louvain-based clustering(38) at varying resolution in different parts of the data manifold as implemented in louvain-igraph (https://github.com/vtraag/louvain-igraph) and adopted by Scanpy. We annotated cell types based on the expression of known marker genes. We merged clusters if only reflecting further heterogeneity within a cell type not discussed in this manuscript. For the exact steps of clustering and annotation and the parameters used consult the available code. In different figures varying resolutions of subtype clustering are shown in this manuscript. We identified characteristic gene signatures of each cluster by testing for differential expression of a single cluster against all other cells using a t-test with overestimated variance implemented in the sc.*tl.rank_genes_groups()* function of Scanpy.

b.4. Differential Expression Testing

We used the MAST(39) package for all single-cell differential expression analyses. MAST uses a two-part linear ('hurdle') model to match the distribution of scRNA sequencing data. We tested differential expression between Dex and Vehicle samples in different subgroups of cells. Firstly, we tested the effect in each of the fine clusters of the iCell8 data individually. Secondly, we investigated the same effect, but instead considering the three coarser cell classes in the iCell8 and 10x data. We included the number of genes expressed in each cell as a covariate in the MAST expression model. To correct for the batch effect of iCell8 individual experiments/chips, we additionally included the chip ID as a covariate in the MAST model for the iCell8 data. After fitting the model we used a likelihood ratio test to test for differential expression between conditions. As an output from MAST we obtained raw p-values, p-values corrected for multiple testing with the Benjamini-Hochberg approach (false discovery rate) and log2 fold changes of gene expression between conditions. We used a false discovery rate ≤ 0.05 as a significance threshold.

b.5. Treatment response in NR3C1-positive vs. -negative cells

To investigate dependence of the Dex response on expression of the GR, we fitted the MAST model as described above for each of the three coarser cell classes in the iCell8 data and obtained log2foldchanges between cells that do or do not express the gene *NR3C1* (GR). As a next step, we intersected the full gene list with genes previously identified to be differentially responsive to Dex in hippocampal progenitors(9). We then used the Wilcoxon signed-ranks test to ask if there was a

significant difference in the response between *NR3C1*-positive and -negative cells in each of the three cell-type groups. Results were deemed significant at a p-value ≤ 0.05. This analysis was only done for cells from all three time-points combined.

b.6. Enrichment analyses

Enrichment analyses were carried out only on the differential expression results of cells from all three time-points combined (iCell8 data) and on cells from the day-90 time point (iCell8 and 10x data).

1. FUMA

Enrichment of differentially-expressed genes against genes carrying SNPs with Genome-Wide Association to a variety of traits was tested using the FUMA algorithm(40) by inputting the various DE gene lists into the GENE2FUNC software. This analysis references the NHGRI-EBI GWAS Catalogue(41) (https://www.ebi.ac.uk/gwas/) most recently updated on 27 May 2019 and containing 943 traits from different studies. We ran an enrichment analysis separately for the DE genes (FDR ≤ 0.05) in the Non-Neural Progenitors, Neural Progenitors, and Neurons cells classes and limited the analysis to traits where 5 or more genes overlapped with the respective test gene sets (corrected p ≤ 0.05). We categorized all traits as 'brain/behaviour' or 'other' in the full list of traits for each cell class where at least one gene was shared. We assessed significant divergence from the 'master' trait list using a Chi square test, with significance set at p ≤ 0.05.

To explore the genes driving these enrichments, we focused on the enriched GWAS terms shared across at least 2 of the Lines1-3 (**Table S16A-B**) specifically in the DEG lists from the Neurons cell classes from day 90 organoids. A total of 107 genes were found to contribute to the significant enrichments (**Table S16C**), with some appearing in multiple terms across multiple cell lines' DEG lists. We counted the number of contributions for each gene and ranked them by this count, from 25 to 1(**Table S16C**).

2. Enrichment analyses for disease-associated genes

To test for enrichment of selected gene-sets in the differentially expressed genes (FDR ≤ 0.05), we used a hypergeometric test as implemented in the package diffxpy (https://github.com/theislab/diffxpy/). We tested for enrichment of all Gene Ontology Biological Function sets (v6.2), obtained from the Molecular Signatures Database(42, 43). We furthermore tested for enrichment of genes sets associated to disease as follows. **(1)** Genes mapping to SNPs with genome-wide significance in the genome-wide meta-analysis of the Cross-Disorder Group of the Psychiatric Genomics Consortium, which included 8 mental illnesses(44) (gene list in **Table S11**). **(2)** Gene sets from the DisGeNET database(45), which includes curated lists of disease-associated genes not only from genetic associations, but also from gene expression analyses and pharmacological studies. Here we focused on two phenotypes: Autism Spectrum Disorders (ASD) and Neurodevelopmental Disorders (ND), and used Height as a non-brain-related phenotype (Gene list in **Table S12**). **(3)** Genes carrying loss-of-function mutations and associated with Intellectual Disability from the most recent Developmental Brain Disorders Database

(DBDB: https://www.dbdb.urmc.rochester.edu/home; Updated March 2019)(10) (gene list in **Table S13**).

We carried out enrichment tests in the following subgroupings: fine clusters individually and each of the three coarse cell classes individually. We applied Benjamini-Hochberg FDR correction on the cluster level (correcting for multiple testing within different groups of cells) as well as on the enrichment list level for the number of compared gene lists when using more than one gene set at once as with sets obtained from the DisGeNET database.

We repeated the above-mentioned enrichment analyses in data from 90-day-old organoids (iCell8 day-90 and 10x day-90 data). Here, we applied an additional log2 fold-change ≥ +/-0.15 threshold on the differential gene expression results besides the FDR ≤ 0.05 filter to compensate the higher sensitivity in the additional differential expression results from the 10x genomics data.

3. Permutation testing of enrichment results

To ensure that enrichment analyses results were not simply reflective of high expression levels of marker genes in particular cell types or classes, we generated 1,000 permutations of equal-sized gene sets that also had the same mean expression distribution as the significant DE gene sets from each cell class (in iCell8 data at day 90 and all three time-points combined and in the 10x day-90 data). The latter was achieved using 5 equal-gene-number bins where the mean gene expression was matched by bin. We then repeated all previous enrichment analyses using each of the permuted genes sets and counted the number of times a p-value ≤ the nominal p-value was reached. We used this to compute empirical p-values and corrected for the number of comparisons (both number of cell types/classes with significant enrichment results to consider, as well as the number of gene lists tested) using Bonferroni correction. Additionally, we repeated the same permutation analysis without binning of genes by expression but randomly sampling the same number of genes from all non-differentially expressed genes as found significantly differentially expressed.

c. Software specifications

For the analysis of the iCell8 data we used Python v3.6.8 with Scanpy v1.4, anndata v0.6.18, h5py v2.9.0 and diffxpy v0.6.3. We used R version 3.6.0 with packages scran v1.12.0, MAST v1.10.0 and BED v1.1.5 with database version with UCB-Human 2019.04.23.

For the analysis of the 10xGenomics data we used Python v3.7.7 with Scanpy v1.4.6, anndata v0.7.1, h5py v2.10.0 and diffxpy v0.7.4. We used R version 3.6.3 with packages scran v1.14.6, MAST v1.12.0 and BED v1.2.3 with database version with UCB-Human 2019.04.23.

We used matplotlib and seaborn to generate figures. Versions of packages required by Scanpy that might influence numerical results are indicated in the custom scripts.

d. Data and code

Primary data and processed data are available at the Gene Expression Omnibus (https://www.ncbi.nlm.nih.gov/geo) as follows: bulk RNA sequencing data are available at GSE181405 and single-cell RNA sequencing data are available at GSE189535. Code for all analyses is available at https://doi.org/10.5281/zenodo.5772643.

Supplementary References

1. Velasco S, Kedaigle AJ, Simmons SK, Nash A, Rocha M, Quadrato G, Paulsen B, Nguyen L, Adiconis X, Regev A, Levin JZ, Arlotta P. Individual brain organoids reproducibly form cell diversity of the human cerebral cortex. Nature. 2019;570:523-527.
2. Yoon SJ, Elahi LS, Pasca AM, Marton RM, Gordon A, Revah O, Miura Y, Walczak EM, Holdgate GM, Fan HC, Huguenard JR, Geschwind DH, Pasca SP. Reliability of human cortical organoid generation. Nat Methods. 2019;16:75-78.
3. Amiri A, Coppola G, Scuderi S, Wu F, Roychowdhury T, Liu F, Pochareddy S, Shin Y, Safi A, Song L, Zhu Y, Sousa AMM, Psych EC, Gerstein M, Crawford GE, Sestan N, Abyzov A, Vaccarino FM. Transcriptome and epigenome landscape of human cortical development modeled in organoids. Science. 2018;362.
4. Kanton S, Boyle MJ, He ZS, Santel M, Weigert A, Sanchis-Calleja F, Guijarro P, Sidow L, Fleck JS, Han DD, Qian ZZ, Heide M, Huttner WB, Khaitovich P, Paabo S, Treutlein B, Camp JG. Organoid single-cell genomic atlas uncovers human-specific features of brain development. Nature. 2019;574:418-+.
5. Nowakowski TJ, Bhaduri A, Pollen AA, Alvarado B, Mostajo-Radji MA, Di Lullo E, Haeussler M, Sandoval-Espinosa C, Liu SJ, Velmeshev D, Ounadjela JR, Shuga J, Wang X, Lim DA, West JA, Leyrat AA, Kent WJ, Kriegstein AR. Spatiotemporal gene expression trajectories reveal developmental hierarchies of the human cortex. Science. 2017;358:1318-1323.
6. Pollen AA, Bhaduri A, Andrews MG, Nowakowski TJ, Meyerson OS, Mostajo-Radji MA, Di Lullo E, Alvarado B, Bedolli M, Dougherty ML, Fiddes IT, Kronenberg ZN, Shuga J, Leyrat AA, West JA, Bershteyn M, Lowe CB, Pavlovic BJ, Salama SR, Haussler D, Eichler EE, Kriegstein AR. Establishing Cerebral Organoids as Models of Human-Specific Brain Evolution. Cell. 2019;176:743-+.
7. Quadrato G, Nguyen T, Macosko EZ, Sherwood JL, Min Yang S, Berger DR, Maria N, Scholvin J, Goldman M, Kinney JP, Boyden ES, Lichtman JW, Williams ZM, McCarroll SA, Arlotta P. Cell diversity and network dynamics in photosensitive human brain organoids. Nature. 2017;545:48-53.
8. Arloth J, Bogdan R, Weber P, Frishman G, Menke A, Wagner KV, Balsevich G, Schmidt MV, Karbalai N, Czamara D, Altmann A, Trumbach D, Wurst W, Mehta D, Uhr M, Klengel T, Erhardt A, Carey CE, Conley ED, Major Depressive Disorder Working Group of the Psychiatric Genomics C, Ruepp A, Muller-Myhsok B, Hariri AR, Binder EB, Major Depressive Disorder Working Group of the Psychiatric Genomics Consortium PGC. Genetic Differences in the Immediate Transcriptome Response to Stress Predict Risk-Related Brain Function and Psychiatric Disorders. Neuron. 2015;86:1189-1202.
9. Provencal N, Arloth J, Cattaneo A, Anacker C, Cattane N, Wiechmann T, Roh S, Kodel M, Klengel T, Czamara D, Muller NS, Lahti J, team P, Raikkonen K, Pariante CM, Binder EB. Glucocorticoid exposure during hippocampal neurogenesis primes future stress response by inducing changes in DNA methylation. Proc Natl Acad Sci U S A. 2019.
10. Mirzaa GM, Millen KJ, Barkovich AJ, Dobyns WB, Paciorkowski AR. The Developmental Brain Disorders Database (DBDB): a curated neurogenetics knowledge base with clinical and research applications. Am J Med Genet A. 2014;164A:1503-1511.

11. Cardenas A, Villalba A, de Juan Romero C, Pico E, Kyrousi C, Tzika AC, Tessier-Lavigne M, Ma L, Drukker M, Cappello S, Borrell V. Evolution of Cortical Neurogenesis in Amniotes Controlled by Robo Signaling Levels. Cell. 2018;174:590-606 e521.
12. Dowey SN, Huang X, Chou BK, Ye Z, Cheng L. Generation of integration-free human induced pluripotent stem cells from postnatal blood mononuclear cells by plasmid vector expression. Nat Protoc. 2012;7:2013-2021.
13. Bruckl TM, Spoormaker VI, Samann PG, Brem AK, Henco L, Czamara D, Elbau I, Grandi NC, Jollans L, Kuhnel A, Leuchs L, Pohlchen D, Schneider M, Tontsch A, Keck ME, Schilbach L, Czisch M, Lucae S, Erhardt A, Binder EB. The biological classification of mental disorders (BeCOME) study: a protocol for an observational deep-phenotyping study for the identification of biological subtypes. Bmc Psychiatry. 2020;20:213.
14. Koyanagi-Aoi M, Ohnuki M, Takahashi K, Okita K, Noma H, Sawamura Y, Teramoto I, Narita M, Sato Y, Ichisaka T, Amano N, Watanabe A, Morizane A, Yamada Y, Sato T, Takahashi J, Yamanaka S. Differentiation-defective phenotypes revealed by large-scale analyses of human pluripotent stem cells. Proc Natl Acad Sci U S A. 2013;110:20569-20574.
15. Okita K, Matsumura Y, Sato Y, Okada A, Morizane A, Okamoto S, Hong H, Nakagawa M, Tanabe K, Tezuka K, Shibata T, Kunisada T, Takahashi M, Takahashi J, Saji H, Yamanaka S. A more efficient method to generate integration-free human iPS cells. Nat Methods. 2011;8:409-412.
16. Lancaster MA, Knoblich JA. Generation of cerebral organoids from human pluripotent stem cells. Nat Protoc. 2014;9:2329-2340.
17. Reul JM, Gesing A, Droste S, Stec IS, Weber A, Bachmann C, Bilang-Bleuel A, Holsboer F, Linthorst AC. The brain mineralocorticoid receptor: greedy for ligand, mysterious in function. Eur J Pharmacol. 2000;405:235-249.
18. Jobe AH, Kemp M, Schmidt A, Takahashi T, Newnham J, Milad M. Antenatal corticosteroids: a reappraisal of the drug formulation and dose. Pediatr Res. 2021;89:318-325.
19. Ballard PL, Ballard RA. Scientific Basis and Therapeutic Regimens for Use of Antenatal Glucocorticoids. Am J Obstet Gynecol. 1995;173:254-262.
20. Sinclair JC. Meta-analysis of randomized controlled trials of antenatal corticosteroid for the prevention of respiratory distress syndrome: discussion. Am J Obstet Gynecol. 1995;173:335-344.
21. Gyamfi C, Mele L, Wapner RJ, Spong CY, Peaceman A, Sorokin Y, Dudley DJ, Johnson F, Leveno KJ, Caritis SN, Mercer BM, Thorp JM, Jr., O'Sullivan MJ, Ramin SM, Carpenter M, Rouse DJ, Miodovnik M, Sibai B, Eunice Kennedy Shriver National Institute of Child H, Human Development Maternal-Fetal Medicine Units N. The effect of plurality and obesity on betamethasone concentrations in women at risk for preterm delivery. Am J Obstet Gynecol. 2010;203:219 e211-215.
22. Andrews S. FastQC: a quality control tool for high throughput sequence data. 2010.
23. Martin M. Cutadapt removes adapter sequences from high-throughput sequencing reads. EMBnet. 2011.
24. Dobin A, Davis CA, Schlesinger F, Drenkow J, Zaleski C, Jha S, Batut P, Chaisson M, Gingeras TR. STAR: ultrafast universal RNA-seq aligner. Bioinformatics. 2013;29:15-21.
25. Fischer DS, Theis FJ, Yosef N. Impulse model-based differential expression analysis of time course sequencing data. Nucleic Acids Res. 2018;46:e119.
26. M.S. B, A. B, G.E. H, S. S, K. B, J.D. B, E. D. Transcriptional signatures of participant-derived neural progenitor cells and neurons implicate altered Wnt signaling in Phelan McDermid syndrome and autism. bioRxiv. 2019.
27. Hoffman GE, Hartley BJ, Flaherty E, Ladran I, Gochman P, Ruderfer DM, Stahl EA, Rapoport J, Sklar P, Brennand KJ. Transcriptional signatures of schizophrenia in hiPSC-derived NPCs and neurons are concordant with post-mortem adult brains. Nature Communications. 2017;8.

28. Ritchie ME, Phipson B, Wu D, Hu YF, Law CW, Shi W, Smyth GK. limma powers differential expression analyses for RNA-sequencing and microarray studies. Nucleic Acids Research. 2015;43.
29. Girardot C, Scholtalbers J, Sauer S, Su SY, Furlong EE. Je, a versatile suite to handle multiplexed NGS libraries with unique molecular identifiers. BMC Bioinformatics. 2016;17:419.
30. Martin M. Cutadapt removes adapter sequences from high-throughput sequencing reads. 2011. 2011;17:3.
31. Liao Y, Smyth GK, Shi W. featureCounts: an efficient general purpose program for assigning sequence reads to genomic features. Bioinformatics. 2014;30:923-930.
32. Godard P, van Eyll J. BED: a Biological Entity Dictionary based on a graph data model. F1000Res. 2018;7:195.
33. Wolf FA, Angerer P, Theis FJ. SCANPY: large-scale single-cell gene expression data analysis. Genome Biol. 2018;19:15.
34. Lun AT, Bach K, Marioni JC. Pooling across cells to normalize single-cell RNA sequencing data with many zero counts. Genome Biol. 2016;17:75.
35. Johnson WE, Li C, Rabinovic A. Adjusting batch effects in microarray expression data using empirical Bayes methods. Biostatistics. 2007;8:118-127.
36. Mayer C, Hafemeister C, Bandler RC, Machold R, Batista Brito R, Jaglin X, Allaway K, Butler A, Fishell G, Satija R. Developmental diversification of cortical inhibitory interneurons. Nature. 2018;555:457-462.
37. Becht E, McInnes L, Healy J, Dutertre CA, Kwok IWH, Ng LG, Ginhoux F, Newell EW. Dimensionality reduction for visualizing single-cell data using UMAP. Nat Biotechnol. 2018.
38. Blondel VD, Guillaume JL, Lambiotte R, Lefebvre E. Fast unfolding of communities in large networks. J Stat Mech-Theory E. 2008.
39. Finak G, McDavid A, Yajima M, Deng J, Gersuk V, Shalek AK, Slichter CK, Miller HW, McElrath MJ, Prlic M, Linsley PS, Gottardo R. MAST: a flexible statistical framework for assessing transcriptional changes and characterizing heterogeneity in single-cell RNA sequencing data. Genome Biol. 2015;16:278.
40. Watanabe K, Taskesen E, van Bochoven A, Posthuma D. Functional mapping and annotation of genetic associations with FUMA. Nat Commun. 2017;8:1826.
41. MacArthur J, Bowler E, Cerezo M, Gil L, Hall P, Hastings E, Junkins H, McMahon A, Milano A, Morales J, Pendlington ZM, Welter D, Burdett T, Hindorff L, Flicek P, Cunningham F, Parkinson H. The new NHGRI-EBI Catalog of published genome-wide association studies (GWAS Catalog). Nucleic Acids Res. 2017;45:D896-D901.
42. Subramanian A, Tamayo P, Mootha VK, Mukherjee S, Ebert BL, Gillette MA, Paulovich A, Pomeroy SL, Golub TR, Lander ES, Mesirov JP. Gene set enrichment analysis: A knowledge-based approach for interpreting genome-wide expression profiles. P Natl Acad Sci USA. 2005;102:15545-15550.
43. Liberzon A, Subramanian A, Pinchback R, Thorvaldsdottir H, Tamayo P, Mesirov JP. Molecular signatures database (MSigDB) 3.0. Bioinformatics. 2011;27:1739-1740.
44. Lee PH. Genome wide meta-analysis identifies genomic relationships, novel loci, and pleiotropic mechanisms across eight psychiatric disorders. bioRxiv. 2019.
45. Pinero J, Bravo A, Queralt-Rosinach N, Gutierrez-Sacristan A, Deu-Pons J, Centeno E, Garcia-Garcia J, Sanz F, Furlong LI. DisGeNET: a comprehensive platform integrating information on human disease-associated genes and variants. Nucleic Acids Res. 2017;45:D833-D839.

Supplementary Figures

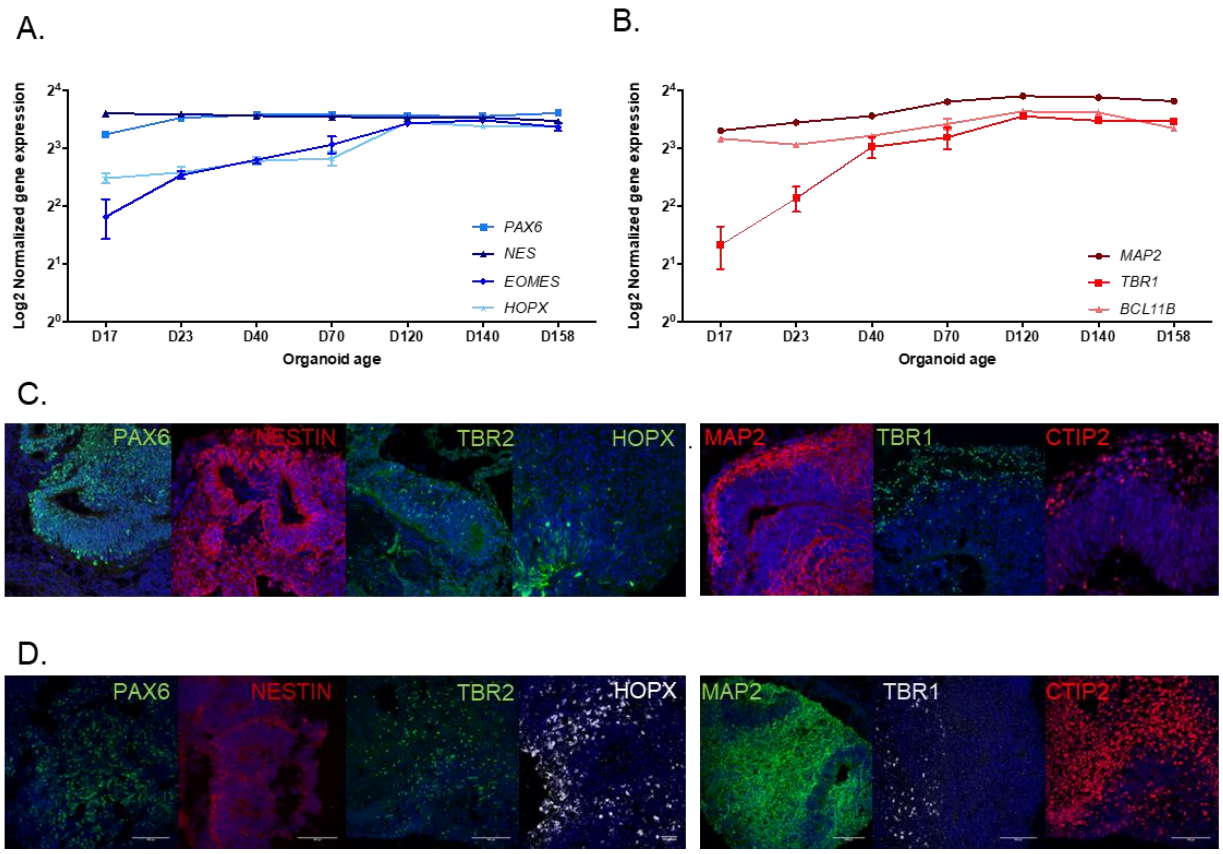

FIGURE S1. Transcriptional characterization of organoids' developmental trajectory. A-B. RNA expression levels of established neural progenitor (**A**) and neuronal (**B**) markers in bulk RNAseq data at days-17-158 in culture. **C-D**. Organoids characterization by known progenitor and neuron markers using immunofluorescence and confocal microscopy at protein expression levels at days 40 (**C**) or 90 (**D**) in culture. Progenitor markers: PAX6 (green), NESTIN (*NES* gene, red), TBR2 (*EOMES* gene, green), HOPX (green in day 40 and grey in day 90). Neuron markers: MAP2 (red in day 40 and green in day 90), TBR1 (green in day 40 and grey in day 90), CTIP2 (*BCL11B* gene, red). For all images in **C-D**, DAPI is used as nuclear marker (blue).

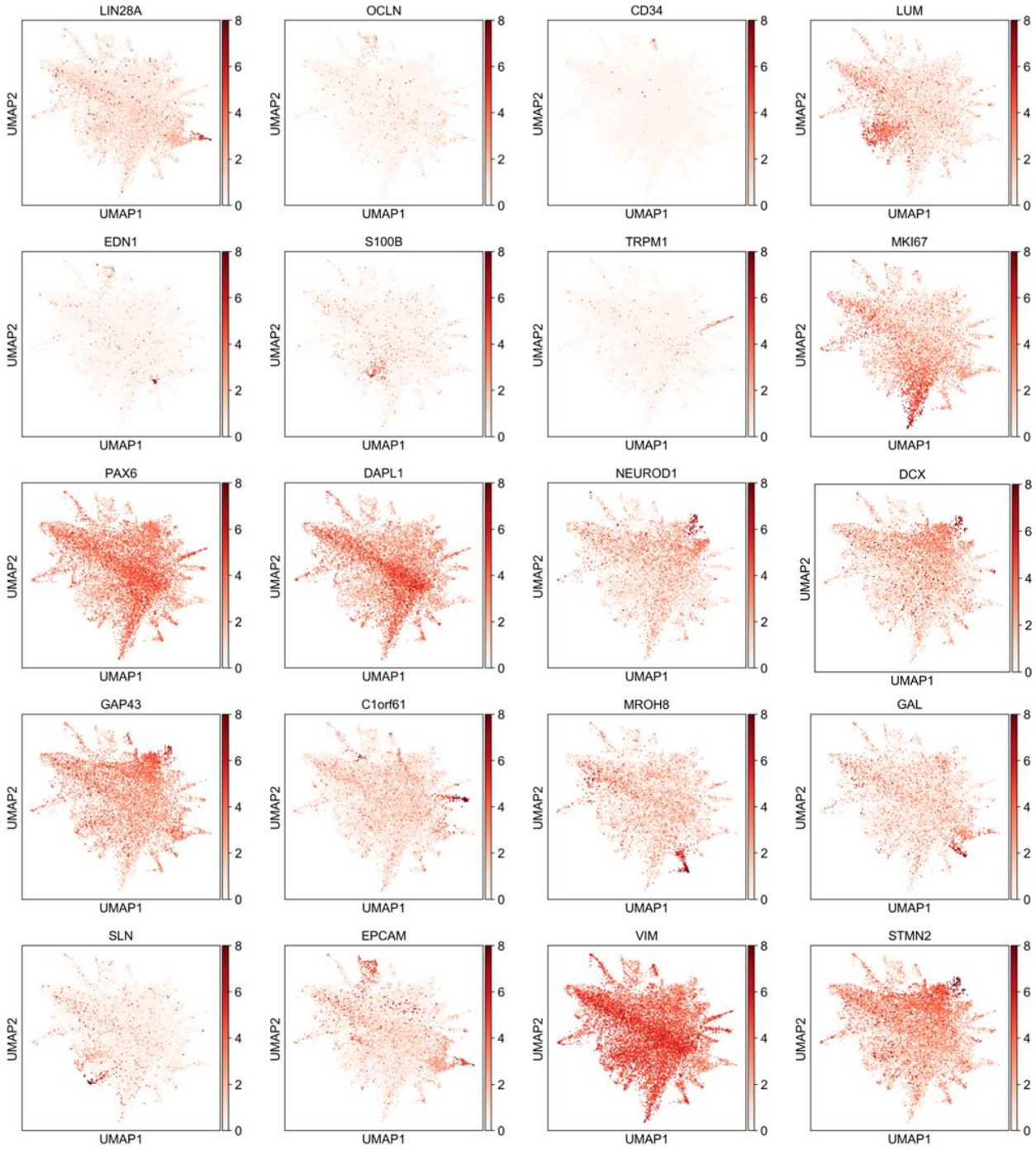

FIGURE S2. UMAPs for cell-types or cell classes from Cell Line 1. *LIN28A*, *OCLN*, *CD34*, *LUM*, *EDN1*, *S100B*, *TRPM1*, *MKI67*, *PAX6*, *DAPL1*, *NEUROD1*, *DCX*, *GAP43*, *C1orf61*, *MROH8*, *GAL*, *SLN*, *EPCAM*, *VIM*, *STMN2* are referenced in dot plot in **Figure S3** for cell-type characterization and cell class characterization.

A.

Code	Full Cluster Name	Cells no.	Sub-group	Cluster markers
NE	Neuroepithelial cells	728	Non-neural Progenitors	*EPCAM, OCLN, LIN28A, ASPM*
ES	Epithelial Stromal cells	299	Non-neural Progenitors	*EPCAM, OCLN, EDN1, CD68, CDH1*
S	Stem cells	70	Non-neural Progenitors	*GNG11, PECAM1, CD34*
M	Mesenchymal Stromal Cells	1177	Non-neural Progenitors	*COL1A2, LUM, DCN*
E	Endothelial cells	26	Non-neural Progenitors	*EDN1*
GP	Glial Precursors	291	Neural Progenitors	*PLP1, S100B, SOX10*
PE	Pigmented Epithelial cells	151	Neural Progenitors	*MITF, PMEL, TRPM1, TMEFF2*
PP	Proliferative Precursors	1510	Neural Progenitors	*TOP2A, MIK67, ASPM*
EP	Early Progenitors / Neuronal Precursors	2240	Neural Progenitors	*PAX6, MIK67, TOP2A, NES, NCAM1*
RG	Radial Glia	2781	Neural Progenitors	*PAX6, SOX2, DAPL1, SIX6, CRABP1*
iN	immature Neurons / Retina	383	Neurons	*NEUROD1, OTX2, CRX, RCVRN*
iDN	immature Dorsal Neurons	2414	Neurons	*STMN2, MAP2, DCX*
DN	Dorsal Neurons	1355	Neurons	*SNAP25, GRIA2, NEUROD6*

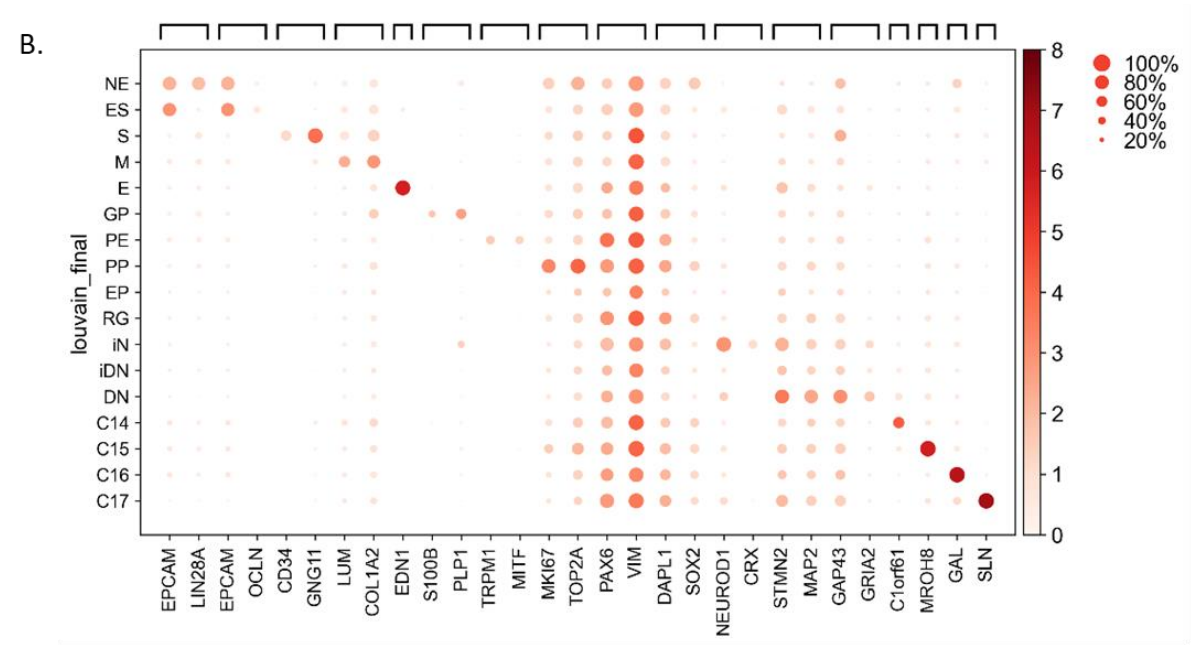

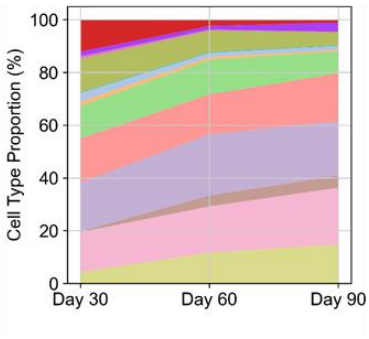

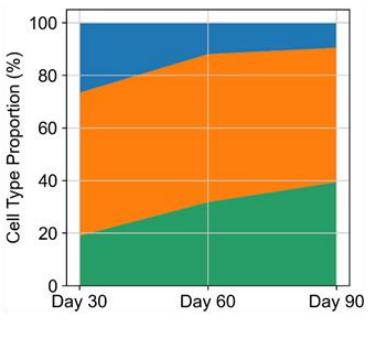

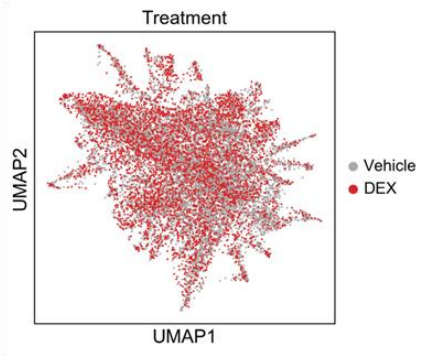

FIGURE S3. Cell-type characterization using single-cell RNA sequencing. A. Definition of the 14 identifiable cell types in developmental order from Neuroepithelial cells (NE, top) to Dorsal Neurons (DN, bottom), abbreviations, number of cells in each cluster, cell class assigned to, and the genes defining each cluster identity. **B.** Dot plot showing the average expression by cluster and

percent of cells expressing each of the top 1-2 genes defining each cluster. **C.** Distribution of total cell numbers by fine cell-types across organoid age (day 30, 60, 90). **D.** Distribution of cell classes across organoid age (day 30, 60, 90). **E**. UMAP plot depicting the cells from organoids that received treatment (red, n=6800 cells) or vehicle (grey, n=7202 cells), showing even distribution of treated/untreated cells.

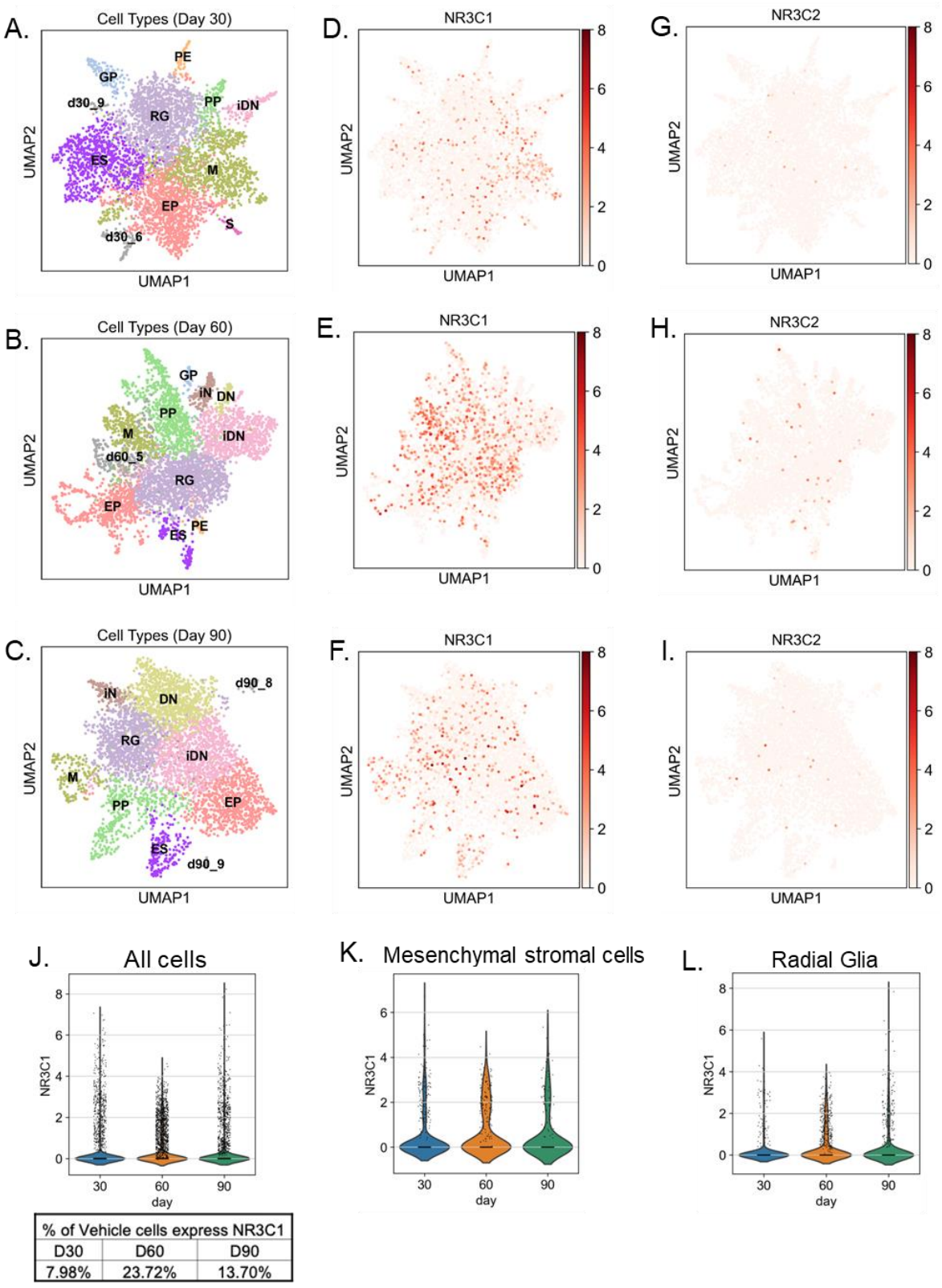

% of Vehicle cells express NR3C1		
D30	D60	D90
7.98%	23.72%	13.70%

FIGURE S4. Cell type characterization by individual days. A-C. UMAP plot of cell-type clustering individually reported for day 30, 60, or 90. **D-F.** UMAP plot of *NR3C1* gene (GR protein) expression individually reported for day 30, 60, or 90. **G-I.** UMAP plot of *NR3C2* gene

(MR protein) expression individually reported for day 30, 60, or 90. **J.** Violin plot of *NR3C1* expression individually reported for day 30, 60, or 90 in all combined cells. Inset table: percent of total cells at each day expressing *NR3C1* at detectable levels. **K-L.** Violin plots of *NR3C1* expression individually reported for day 30, 60, or 90 in individual cell types of interest: **K**, Mesenchymal cells (M) clusters; **L**: Radial Glia (RG) cells clusters.

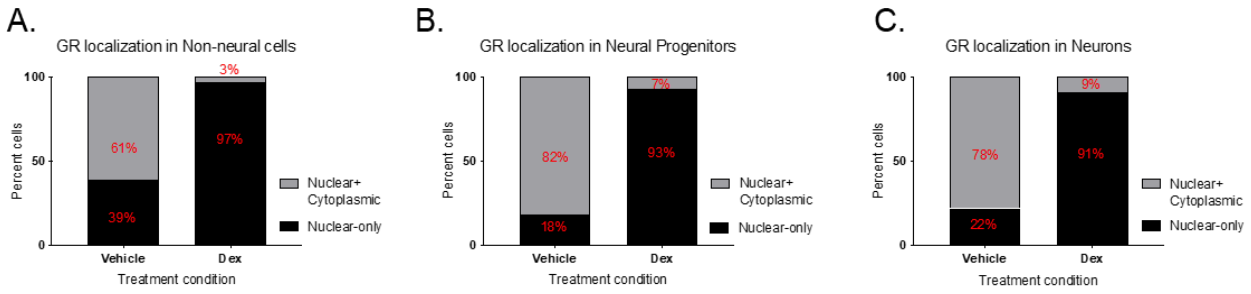

FIGURE S5. Quantification of nuclear translocation of GR protein following Dex treatment, in Non-Neural Cells (**A**), Neural Progenitors (**B**) and Neurons (**C**).

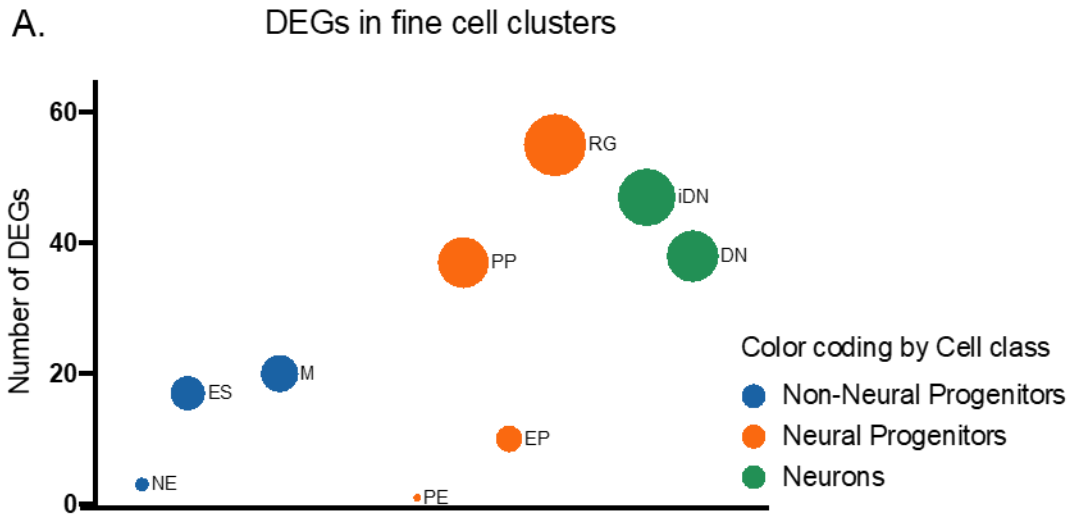

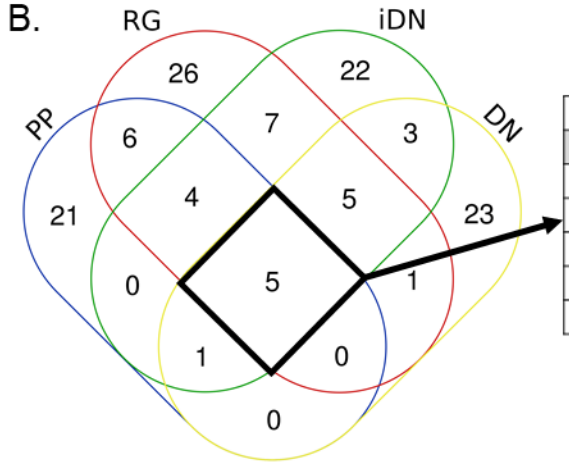

	Absolute Fold Change			
Gene	PP	RG	iDN	DN
MGARP ↑	1.765	1.983	1.540	1.331
C1orf61 ↓	0.335	0.397	0.456	0.361
LINC01551 ↓	0.273	0.513	0.516	0.339
NEUROD6 ↓	0.355	0.448	0.318	0.175
NFIA ↓	0.492	0.564	0.428	0.312

FIGURE S6. Cell-type-specific differential gene expression in organoids. **A.** Differential gene expression by single-cell cluster. Bubble plots show number of differentially-expressed genes (DEGs; y-axis) by average *NR3C1* expression (x-axis) in all 9 clusters with at least one significant DEG. **B.** Venn diagram depicting the intersection between lists of DE genes for the top four clusters by number of DE genes (PP, RG, iDN, and DN). The 5 genes shared by all four clusters are highlighted in the table along their differential expression fold change for each cluster.

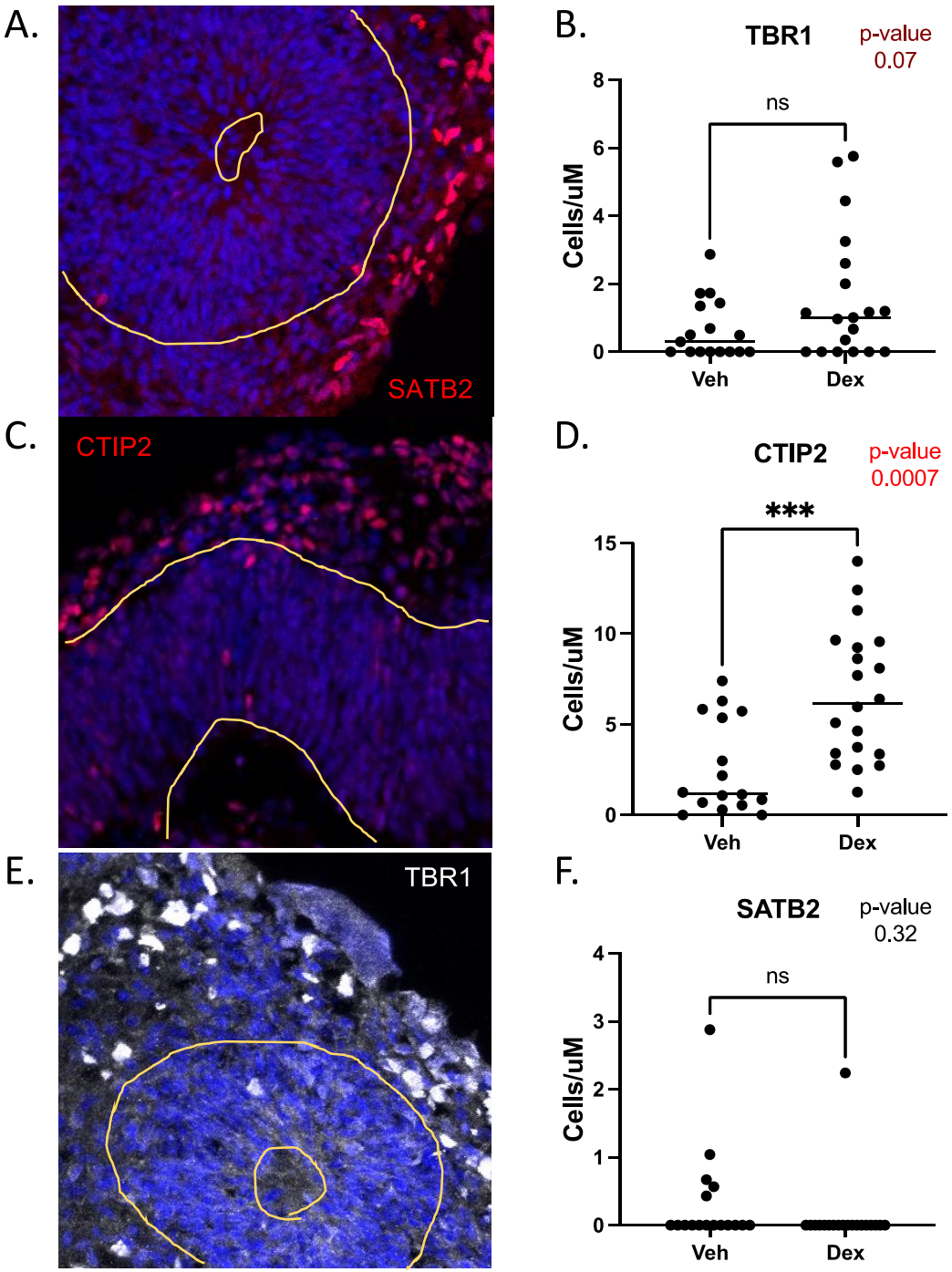

FIGURE S7. Increased formation of new neurons 8 days removal of acute (12hr) Dexamethasone (Dex) stimulation. Immunofluorescence staining was performed in organoids aged 60 days with 100nM Dex or vehicle control (DMSO). After 12 hours, the treatment media was replaced with wild-type conditions, and organoids were grown for an additional 8 days. Following confocal microscopy imaging of 17-20 ventricles per condition, ventricular zones were marked, and TBR1-, CTIP2-, and SATB2-positive cells were counted. Counts were normalized by ventricular area, as there was no difference in density of DAPI-positive nuclei between Dex and Vehicle. Group differences were compared using unpaired t-tests.

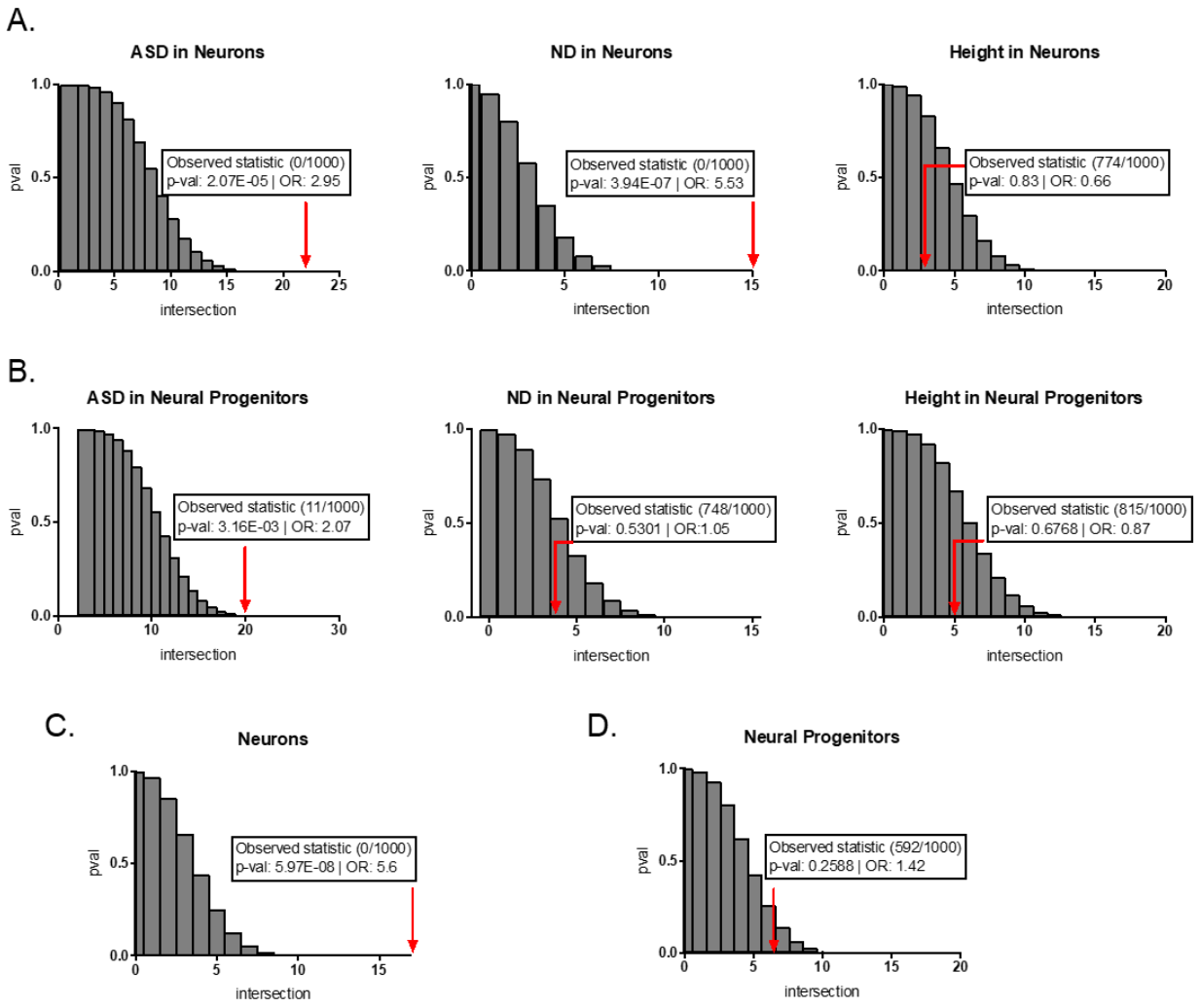

FIGURE S8. A-B. Permutations (n=1000) of DGN gene lists enrichment test in mean-matched non-significant (q-value >0.05) genes from Neurons (**A**) or Neural Progenitors (**B**) DE analyses. **C-D.** Permutations (n=1000) of DBDD intellectual disabilities enrichment test in Mean-matched non-significant (q-value >0.05) genes from Neurons (**C**) and Neural Progenitors (**D**) or DE analyses.

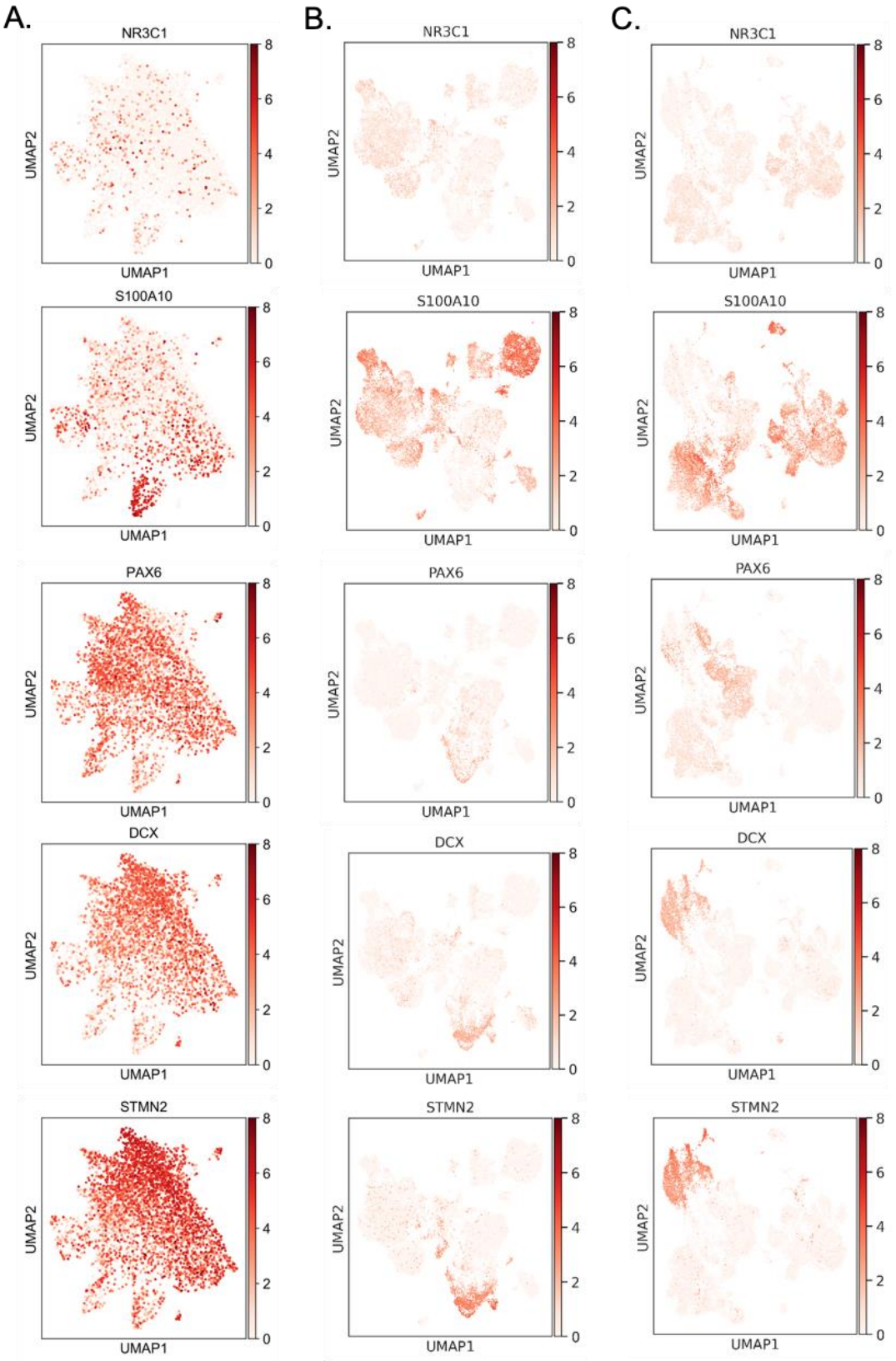

FIGURE S9. UMAP graphs of expression of cell-class-specific genes in Line1 (**A**), Line2 (**B**) and Line3 (**C**) –derived single cell transcriptomes.

Supplementary Table Legends (supplementary tables appear in a separate document, appi.ajp.2021.21010095.ds002.xlsx)

Table S1: Bulk RNAseq counts matrix. Batch-corrected and normalized gene expression counts for each of 21 RNAseq libraries, following ImpulseDE2 analysis. Genes in Column 1 are presented as Ensembl IDs. Each library/sample name is presented as "DayX_replicate".

Table S2: ImpulseDE2 results depicting genes that peak (significantly different from the other days) at each organoid developmental time point. Genes' normalized expression levels are represented visually in **Figure 1A** via a heatmap.

Table S3: Quantitative PCR differential expression after dose-time experiment in bulk organoids at day 45 in culture. Treatment was done in the medium with Dexamethasone dissolved in DMSO (10nM, 100nM, and 1000nM concentrations). The vehicle condition was DMSO. Triplicate biological experiments were used for the treatment, and the qPCR analyses were run in quadruplicate technical replicates. Analysis of qPCR data was done using the absolute quantification method.

Table S4: Cluster markers - cell types and cell classes.

Table S5: Significant DE results for **day-30** organoids, based on cluster classification (in 13 named cell-type clusters) and cell class (in 3 cells classes).

Table S6: Significant DE results for **day-60** organoids, based on cluster classification (in 13 named cell-type clusters) and cell class (in 3 cells classes).

Table S7: Significant DE results for **day-90** organoids, based on cluster classification (in 13 named cell-type clusters) and cell class (in 3 cells classes).

Table S8: Significant differentially-expressed genes from **Alldays** combined analysis, based on cluster (in 9 named cell-type clusters with significant results) and cell class (in 3 cells classes) classification.

Table S9: Annotation of DEGs shared by non-Neural Progenitors, Neural Progenitors, and Neurons in **Alldays** analysis. Gene ontology analysis in DE genes from three cell classes. Enrichment tested against Biological Process (BP) GO terms and multiple testing corrections performed using Benjamini-Hochberg correction against number of terms and number of test genes sets.

Table S10: DEGs from **Alldays** analyses now repeated to include log2FC and q-values from the individual analyses at Day30, Day60 and Day90 from Table S8. Counts of each time a day-specific result had a log2FC value in the opposite direction from **Alldays** and also was significant (q-value $\leq$0.05). The most frequent direction switch happens in the NP DEGs at day 30 with 2.2% genes

switching. In neither of the three cells classes DEGs does direction change in any gene in any more than one age.

Table S11: FUMA GWAS enrichment results. GWAS-significant traits with 5 or more overlapping genes to the test gene set (DE after Dex in Non-Neural Progenitors, Neural Progenitors or Neurons in organoids) were included in the enrichment analysis. Benjamini-Hochberg multiple testing correction was done for each test gene set against the number of traits included in analysis.

Table S12: Enrichment analyses of psychiatric disease-related gene sets associated genome-wide significant common variants from the genome-wide meta-analysis of the Cross-Disorder Group of the Psychiatric Genomics Consortium.

Table S13: Enrichment analyses of neurodevelopmental disease-related gene sets from the DisGeNET database.

Table S14: Enrichment of genes with Loss-of-Function mutation associated with Intellectual Disability from the Developmental Brain Disorders Database (DBDD) genes database (last updated Mar 2018).

Table S15: Significant DE results for **day-90** organoids derived from validation cell Lines 1 and 2, based on cell class (in 3 cells classes).

Table S16: FUMA GWAS enrichment results for validation datasets at **day 90**. GWAS-significant traits with 5 or more overlapping genes to the test gene set (DE after Dex in Neurons from organoids derived from Lines1-3 at 90 days in culture) were included in the enrichment analysis. Benjamini-Hochberg multiple testing correction was done for each test gene set against the number of traits included in analysis.

Table S17: Shared genes driving significant enrichment of GWAS terms across Lines1-3 neurons DEGs. **A.** Significant GWAS terms shared across all from the FUMA analysis (Table S15) shared by at least two of the 3 Lines (n=12), and the genetic background in which it as identified. Only 'Irritable mood' was shared across all three, while 11 other terms were shared by two enrichment analyses. **B.** Genes associated with the 'Irritable mood' GWAS. **C.** Genes associated with any of the 12 terms (n=107 genes), including the number of total contributions of each gene to enrichments across the analyses for the three datasets from neurons in Line1- 3, the log2 fold-change values for each of the three neurons analyses (Line1, 2, 3), and gene annotations.

Table S18: Enrichment analyses of psychiatric disease-related gene sets associated genome-wide significant common variants from the genome-wide meta-analysis of the Cross-Disorder Group of the Psychiatric Genomics Consortium (upper) and genes with Loss-of-Function mutation associated with Intellectual Disability from the Developmental Brain Disorders Database (DBDD) genes database (lower). Results from Lines 1-3 at **day-90** organoids.